

# Feasibility theory reconciles alternative approaches to neuromuscular control

Brian A. Cohn<sup>a,1</sup>, May Szedlák<sup>b,1</sup>, Bernd Gärtner<sup>b</sup>, and Francisco J. Valero-Cuevas<sup>c,d</sup>

<sup>a</sup>University of Southern California, Department of Computer Science, Los Angeles, CA, USA; <sup>b</sup>ETH Zurich, Department of Theoretical Computer Science, Zurich, Switzerland; <sup>c</sup>University of Southern California, Department of Biomedical Engineering, Los Angeles, CA, USA; <sup>d</sup>University of Southern California, Division of Biokinesiology and Physical Therapy, Los Angeles, CA, USA

This manuscript was compiled on August 20, 2017

We present a conceptual and computational framework to unify today's theories of neuromuscular control called feasibility theory. We begin by describing how the musculoskeletal anatomy of the limb, the need to control individual tendons, and the physics of a motor task uniquely specify the family of all valid muscle activations that accomplish it (its 'feasible activation space'). For our example of static force production with a finger with seven muscles, computational geometry characterizes, in a complete way, the structure of feasible activation spaces as 3-dimensional polytopes embedded in 7-D. The feasible activation space for a given task is the landscape where all neuromuscular learning, control, and performance must occur. This approach unifies current theories of neuromuscular control because the structure of feasible activation spaces can be separately approximated as either low-dimensional basis functions (synergies), high-dimensional joint probability distributions (Bayesian priors), or fitness landscapes (to optimize cost functions).

Neuromechanics | Motor Control | Tendon actuation | ...

This PNAS journal template is provided to help you write your work in the correct journal format. Instructions for use are provided below.

How the nervous system selects specific levels of muscle activations (i.e. a muscle activation pattern) for a given motor task continues to be hotly debated. Some suggest the nervous system either combines low-dimensional synergies (1–7), learns probabilistic representations of valid muscle activation patterns (8–11), or optimizes physiologically-tenable cost functions (12–17). At the core of this problem lies the nature of 'feasible activation spaces,' and the computational challenge of describing and understanding their high-dimensional structure (for an overview, see (18)). A feasible activation space is the family of valid solutions (i.e. muscle activation patterns) available to the nervous system to produce a given motor task. Fig. 1 illustrates the neuromechanical interactions that define the feasible activation space for a particular task.

The most the nervous system can do, therefore, is select a specific muscle activation pattern from within the feasible activation space—as muscle activation patterns outside of this space are, by definition, inappropriate for the task. In fact, the feasible activation space defines the landscape upon which all neuromuscular learning and performance must occur. Understanding neuromuscular control is, therefore, equivalent to understanding how the nervous system finds, explores, inhabits, and exploits the structure of feasible activation spaces (1–6, 22).

But the 'curse of dimensionality' (23–25) makes it computationally challenging to calculate, describe, and understand the nature and structure of high-dimensional feasible activation spaces (4, 12, 19, 20, 26–28)—even for an isolated human fin-

ger or cat leg generating everyday static forces (1, 18, 29, 30). This is due to the computational complexity of algorithms applied upon high dimensional spaces.

Current theories of neuromuscular control are alternative responses to the curse of dimensionality, which at times can be seen as competing, rather than complementary. However, the fundamental neuromechanics of the limb and the physics of the task are the common ground for all theories. Thus, understanding the nature and structure of feasible activation spaces would help compare, contrast and combine these alternative approaches to neuromuscular control.

We now propose a conceptual and computational framework to provide complete characterizations of feasible activation spaces, thereby contextualizing and unifying multiple theories of neuromuscular control. As an example, we leverage prior work (1, 21, 31) to now describe the structure of the feasible activation space for the seven muscles of the index finger when producing static fingertip force. This is the type of fingertip force observed when, for example, pressing hard on a table without finger movement, and is also referred to as an isometric force task. In this case, the feasible activation space is a polytope embedded in 7-dimensional muscle activation space. A polytope is the name given to bounded convex polyhedra in dimensions higher than 3. Our computational approach hinges on the efficient sampling and complete representation of the structure of high-dimensional polytopes. This then characterizes all valid muscle activation patterns. These computational techniques can scale up to ~40 dimensions, which suffices to analyze the neural control of all muscles in a extant vertebrate limb systems. By providing a complete characterization of all muscle activation patterns for a given motor task, we are able

## Significance Statement

Wings take flight, eyes refract light, and muscles manipulate bones within the interplaying constraints of Newtonian physics. Here we apply the basic tenets of physics to the field of neuromechanical control, to elucidate the neuro-physical-motor landscape upon which evolution and learning operate. With three interweaving hypotheses of motor control in the literature, we fill the gap between the disparate approaches by recontextualizing the problem of force control as a physical constraints problem, thereby lighting the stage of optimal, synergistic, and bayesian control.

Please provide details of author contributions here.

Please declare any conflict of interest here.

<sup>1</sup>A.O.(Author One) and A.T. (Author Two) contributed equally to this work (remove if not applicable).

<sup>2</sup>To whom correspondence should be addressed. E-mail: author.two@email.com

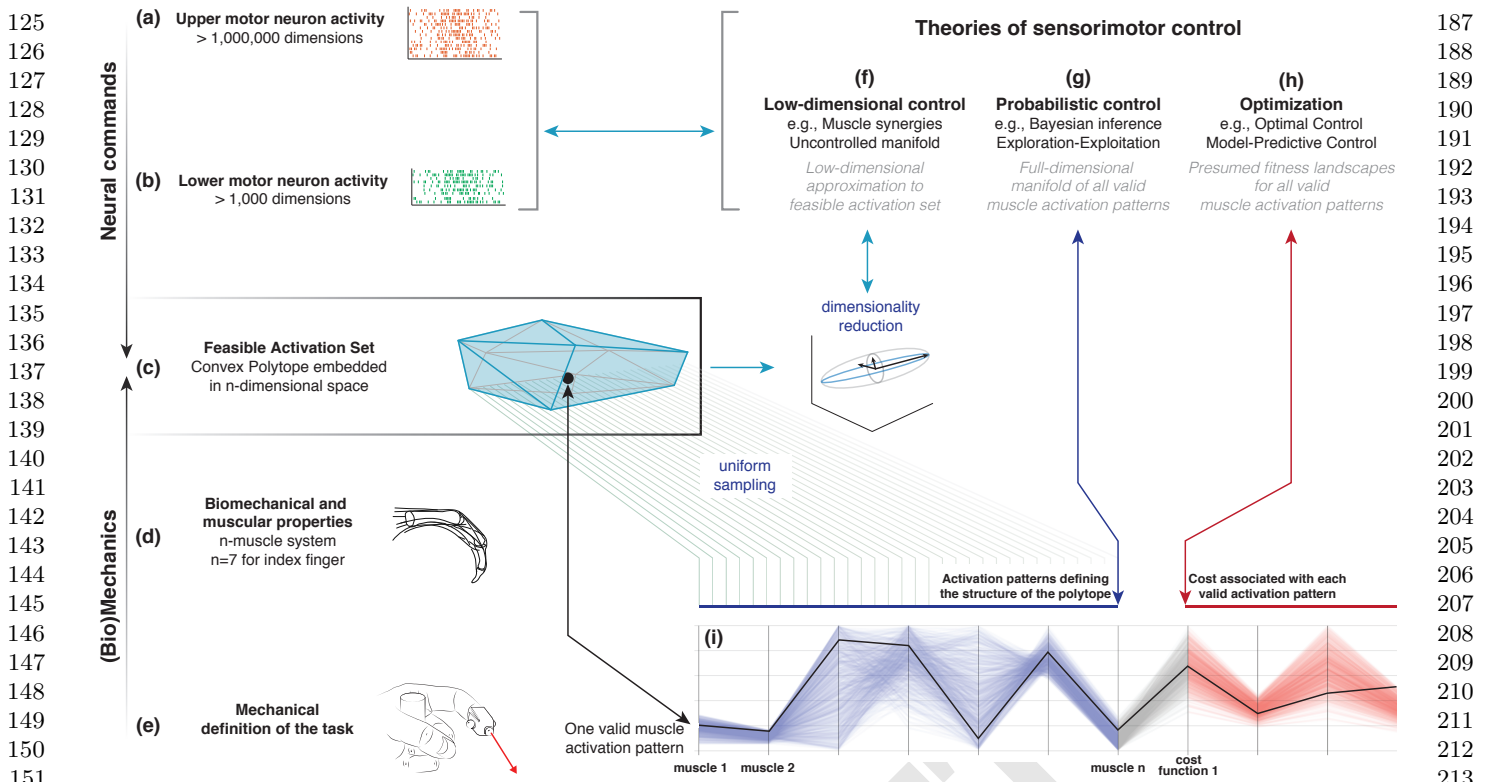


**Fig. 1. Feasible activation spaces guiding sensorimotor control of a task.** The descending motor command for a given task is issued by the primary motor cortex (a), which projects onto alpha-motor neuron pools in the spinal cord (b). The combined drive to all alpha-motor neurons of a muscle can be considered its total muscle activation level (a value between 0 and 1). If we consider that motor commands are sent to multiple independently controlled muscles, then the overall motor command can be conceptualized as a multi-dimensional muscle activation pattern (i.e., a point) in a high-dimensional muscle activation space (12, 19–21) (c). For that muscle activation pattern to be valid, it has to elicit muscle forces (d) capable of satisfying the mechanical requirements of the task—in this case a well directed fingertip force (e). Given the large number of muscles in vertebrates, there is muscle redundancy; there is a large number of valid muscle activation patterns that can produce a given task. We propose that our novel ability to characterize the high-dimensional structure of feasible activation spaces (i) allows us to compare, contrast and reconcile today's three dominant approaches to redundancy in sensorimotor control (f, g, h).

to compare, contrast, combine—and reconcile—today's three dominant approaches to neuromuscular control.

## Results

The goal of this work is to use different perspectives to describe the high-dimensional structure of these feasible activation spaces; we then show how these spaces allow us to unify today's theories of neuromuscular control. We used our realistic index finger model to calculate the feasible activation space for the task of producing static fingertip force in the distal direction (see Fig. 1). The model represents each muscle's contribution to fingertip force as a directed force vector at the fingertip; there are 7 of these force vectors at the index fingertip. As described briefly in the Methods, Hit-and-Run is a method in polytope sampling that we use to sample from the infinite number of muscle activations within the feasible activation space. In effect, given a fingertip task force and the maximum linear fingertip forces each muscle creates, we can collect the muscle activations required to produce that task. As we can now collect thousands of muscle activation patterns for any isometric force task, we examined how the feasible activation spaces (and their representations) change with increasing task intensity in the distal direction (Fig. 1e).

We collected points for multiple task intensities between 0% (i.e., pure co-contraction without output force) and 100%

of maximal static force.

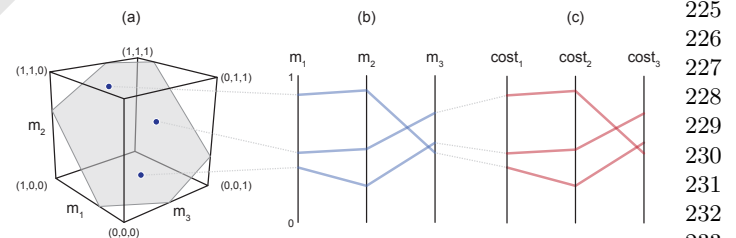


**Fig. 2. Characterizing the high-dimensional structure of a feasible activation space via parallel coordinates.** Consider three points (i.e., muscle activation patterns in Supplemental Fig. ??e) from the feasible activation space (a). The activation level for each muscle (i.e., the coordinates of each point) are sewn across three vertical parallel axes (b). As is common when evaluating multiple valid coordination patterns, each point can be assigned a cost as per an assumed cost function. The associated cost for each muscle activation pattern can also be shown as an additional dimension. We show three representative cost functions (c). Activation levels are bound between 0 and 1, and costs are normalized to their respective observed ranges.

**Parallel coordinate visualization naturally reveals the structure of the feasible activation space.** We used Hit-and-Run to sample from feasible activation spaces for 6 task intensities, labeled as task intensities  $\alpha$  of 0.0, 0.2, 0.4, 0.6, 0.8 and 1.0. For each task intensity, we ran 100,000 Hit-and-Run iterations and

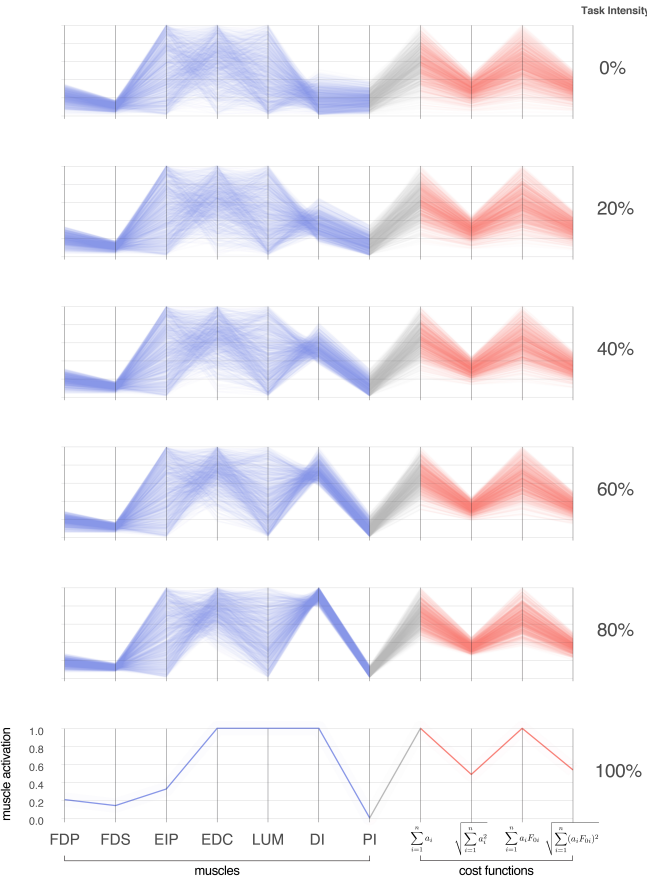


**Fig. 3. Activation patterns of the seven muscles of the index finger across six magnitudes of a fingertip force** The connectivity across parallel coordinates shows how muscle activation patterns are related in multiple ways to produce a fingertip force vector between 0 (a) to 100% (f) of maximal magnitude. At these extremes we have, respectively, the coordination patterns that produce pure co-contraction and the one unique solution for maximal output. In between, we see the how the structure of the feasible activation spaces changes as redundancy is lost. In blue are the activation values, and in red are normalized costs for four cost functions common in the literature. *FDP*: flexor digitorum profundus, *FDS*: flexor digitorum superficialis, *EIP*: extensor indicis proprius, *EDC*: extensor digitorum communis, *LUM*: lumbrical, *DI*: dorsal interosseous, *PI*: palmar interosseous.

down-sampled to every 100<sup>th</sup> point to produce 1,000 points that are (in our experiments) uncorrelated and uniformly distributed in  $P$ . Recall that approaching 100% of maximal force shrinks  $P$  to a single, unique solution (? ).

Parallel coordinate visualization effectively reveals correlations that exist among the 1,000 valid muscle activation patterns for each magnitude of desired fingertip force, and activation pattern cost, Fig. 2 and Fig. 3.

An interactive parallel coordinate visualization plot can be accessed at <https://briancohn.github.io/space-parcoords/>. This interactive interface for parallel coordinate visualization allows us to explore subsets of the valid muscle activation patterns.

For example, restricting the range of muscle activation of one or more muscles shows us the necessary activation levels of the remaining muscles. This can be used to, say, simulate a 40% reduction in possible activation to some muscles (e.g., due to a peripheral neuropathy) in the extrinsic extensor muscles of the index finger innervated by the radial nerve (EIP and EDC) (32).

Figures in the Supplemental Material show how, for 80% of task intensity (i.e., 80% of maximal force output), only 29% (i.e.,  $\frac{290}{1,000}$ ) of all possible solutions survive when capping the maximal excitation of EIP and EDC at 60%. Thus, any neural or muscle dysfunction that compromises the ability of the extensor muscles will limit the choices the nervous system has to produce this force—even at sub-maximal levels. These results further challenge the notion of muscle redundancy as discussed in detail in (18, 33).

Moreover, this same case of task intensity of 80% and maximal excitation of EIP  $\leq$  60% reveals important and counterintuitive consequences in the control of musculature. For example, the range of feasible activation level for some muscles do not change too much (FDP, FDS, and LUM), but does change for others (DI and PI). Most interestingly, the range of costs across valid solutions remains broad.

Similarly, we can describe any subset of muscle activation patterns associated with specific ranges for a given cost function. Figures in the Supplemental Material also show how can characterize all muscle activation patterns associated with the lowest 10% of L2 weighted costs. The coordination patterns that meet this strict criterion are quite different from one another (note the broad ranges and criss-cross patterns).

These relationships among all valid 7-dimensional muscle activations patterns reveal important aspects of the structure of the feasible activation space, and its associated cost landscapes. We see one muscle can affect other muscles in different ways: while limiting PI to 20% of maximal activation eliminates 30.1% of the valid solutions, limiting DI to 20% eliminates 42.8% of them. Similarly we can distinguish between changes in the extreme values of muscle activation from changes in the number of valid solutions. Consider the range of activation for DI and PI at task intensity of 80% which lies between 0 and 0.52 and 0.39, respectively. Limiting DI to 20% pulls PI's maximum down by nearly 0.20, and the converse has nearly the same effect. However, in both cases, the median activation among surviving solutions changes no more than 0.06. This emphasizes that understanding feasible activation spaces requires and understanding of its internal density and not just its bounds. The density of **between-muscle** connec-

373 tivity is seen directly by the density of the lines connecting  
374 the different muscles and cost functions. The **within-muscle**  
375 density can be computed by binning points at each activation  
376 level value.

377     Lastly, those same connecting lines in the parallel coordinate  
 378 visualization allow us to characterize the interrelatedness  
 379 of valid solutions in 7-dimensional space. For example, the  
 380 lines connecting FDP and FDS are mostly parallel, indicating  
 381 a strong positive correlation. In fact, looking at these lines  
 382 allows one to directly see and understand the Pearson product-  
 383 moment correlation coefficients of 0.99, -0.50, and -0.06 in the  
 384 adjacent muscle pairs FDP—FDS, LUM—DI, and EIP—EDC,  
 385 respectively. The interactive parallel coordinate visualization  
 386 also allows for any pairwise comparison by simply dragging  
 387 and reordering the vertical axes—and hovering over individual  
 388 data rows highlight an individual valid activation pattern atop  
 389 all others.

**391 Low-dimensional approximations to the feasible activation**  
**392 space.** We applied PCA (Principal Component Analysis) to

**space.** We applied PCA (Principal Component Analysis) to the valid muscle activation patterns sampled uniformly at random from the feasible activation space. We show results for 10 levels of task intensity. However, we did this in an iterative fashion to replicate the fact that experimental studies can only collect a finite amount of data from each subjects. Thus, from the total pool of 10,000 sub-sampled points sampled by Hit-and-Run (i.e., accepting every 100th point from 100,000 total samples to remove potential autocorrelation among points); sample sizes of 10, 100, and 1,000 points (i.e., simulated ‘experimental’ sample sizes) were replicated 100 times each. We applied PCA to each set of sampled points.

The variance explained by PC1 and PC2 (and its boxplot distribution) for all iterations are shown to change with task intensity for all sample sizes (Fig. 5). Explaining about 13-15% of the variance, PC3 is exactly equal to the remaining variance not explained by the first two components—this is a result of the feasible activation space being a 3-dimensional polytope  $P$  by construction (i.e., recall that 4 task constraints applied to 7 muscles produce a 3-dimensional polytope embedded in the 7-dimensional muscle activation space).

The boxplots in Fig. 5 quantify how different amounts of data change the estimates of variance explained by PC1 and PC2 with task intensity (c.f. labels a vs. b vs. c). We see this dispersion is small in the center and right columns. Note that the ratio of variance explained between PC1 and PC2 between 50 to 80% of task intensity is indicative of changes in the aspect ratio of the feasible activation space—which we see changes with task intensity.

Importantly, using experimentally realistic samples sizes of 10 repetitions per subject (leftmost column) not only does not capture this change, but its standard deviation is large enough to blur the statistically significant differences that are known to appear with larger (but experimentally unrealistic) sample sizes. The impact of impoverishing the number of samples fed to PCA reminds us that inadequate amounts of data obfuscate the underlying changes in the structure of the data analyzed (Fig. 5).

430 There were also important changes in the loadings of the  
 431 PC1 and PC2 vectors. While the ratio of variance explained  
 432 between PC1 and PC2 gives a sense of the aspect ratio of  
 433 the feasible activation space, the loadings of PC1 and PC2  
 434 speak to its orientation. Fig. 6 shows how the loadings of

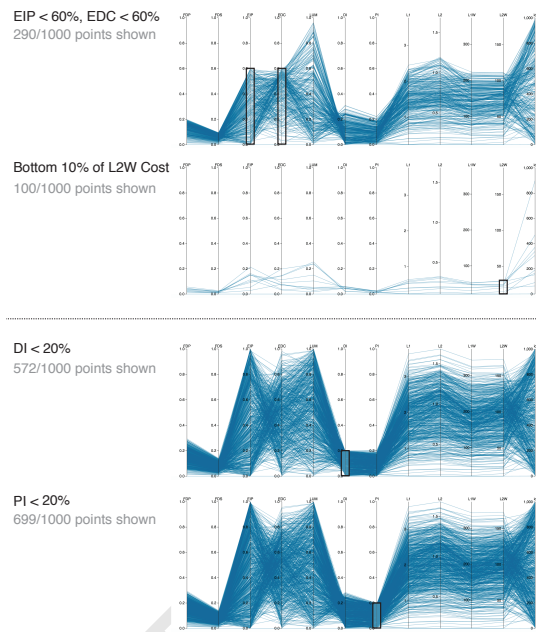


**Fig. 4. Supplemental Figure: Posthoc constraints on a task intensity of 80%**  
 Here we show four unique examples of constraints applied to the points collected from the feasible activation space. With this, we can rapidly predict how index finger control must change in the event of weakness in specific muscles. We also can see how many points remain once the constraints are added—signaling how the structure of the feasible force space is affected.

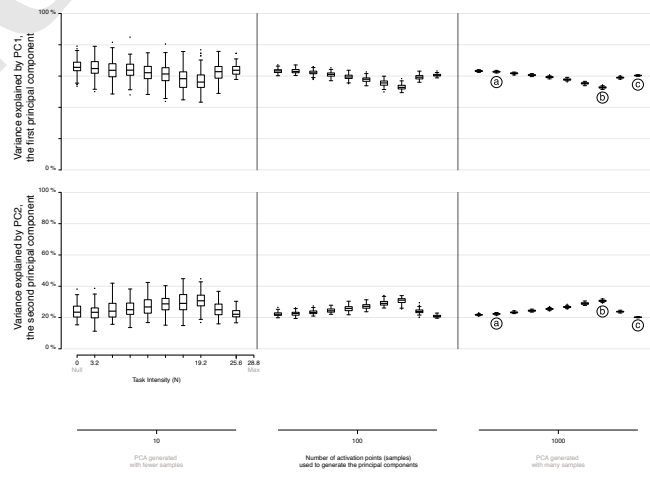


**Fig. 5. Approximating the structure of feasible activation spaces via principal components analysis (PCA) is sensitive to both the number of points used and the intensity of the task.** Rows show the variance explained by the first (top) and second (bottom) principal components with increasing data points (left to right). It is not possible to generalize the variance explained across tasks intensities, and large numbers of points (i.e., > 100) are needed to confidently estimate the real changes in variance explained as a function of task intensity (cf. points labeled a, b, c).

497 the PC1 and PC2 vectors change across labels a, b, and c  
498 (Fig. 5) corresponding to 11, 66 and 88% of task intensity,  
499 respectively. What these loadings indicate are the direction in  
500 7-dimensional space, which changes dramatically.

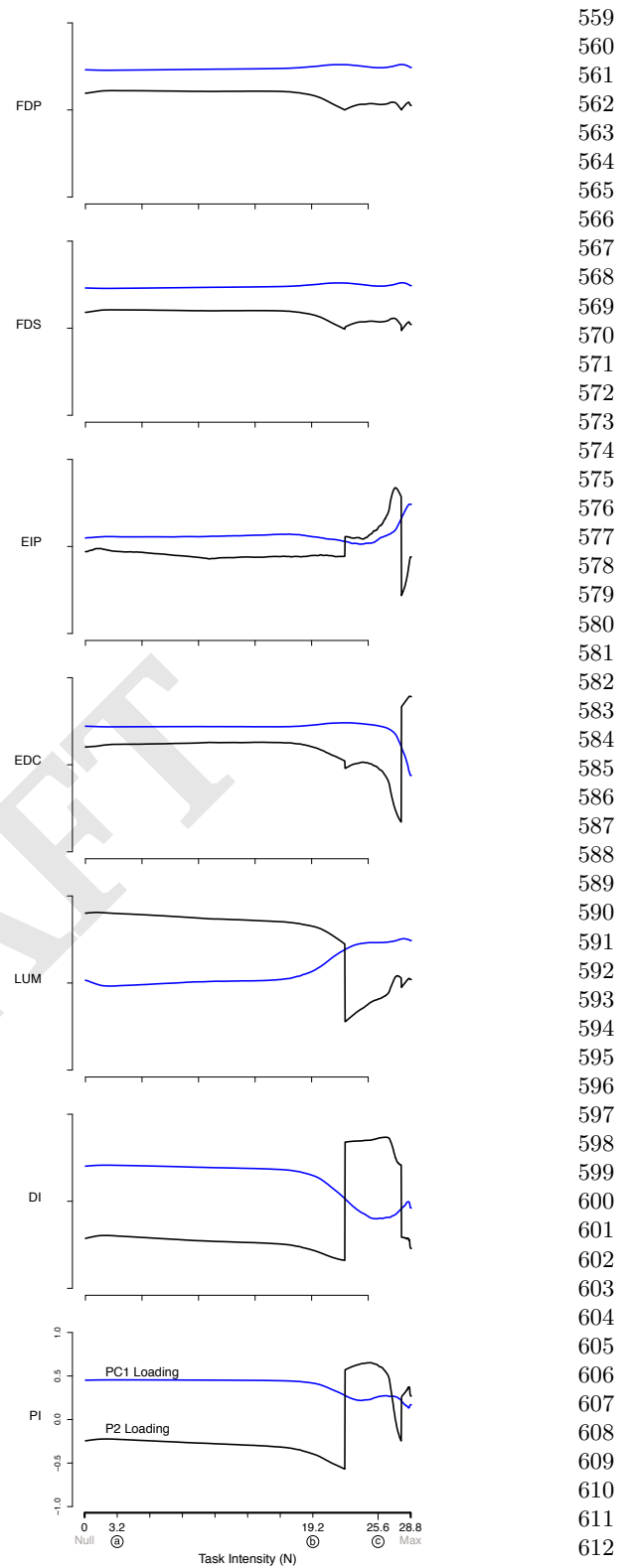
501 These changes we see in (i) the lower and upper bounds of  
502 activations, and in (ii) the relative variance explained and (iii)  
503 loadings for PC1 and PC2, demonstrate that the size, shape  
504 and orientation of the feasible activation space changes with  
505 task intensity. Moreover, these changes represent the best-case  
506 scenario given the absence of experimental noise, within- and  
507 across-subject variability, and measurement error.

508 **Changes in the probabilistic structure of the feasible activation**  
509 **space with increasing task intensity, or how muscle re-**  
510 **dundancy is lost.** The maximal static fingertip force vector in  
511 a given direction is produced by a single and unique combina-  
512 tion of muscle activations. In contrast, any sub-maximal mag-  
513 nitude of that same vector is produced by an infinite number  
514 of solutions (12, 18, 19, 34). Our analysis of feasible activation  
515 spaces at different task intensities allows us to characterize how  
516 this redundancy changes and is lost. The histogram heatmaps  
517 in Fig. 7 illustrate the changes and shrinking of within-muscle  
518 density of valid activation levels for sub-maximal forces, con-  
519 verging to a single solution for maximal force output. These  
520 surface plots show how the normalized histograms (of 1,000  
521 valid activation levels for each muscle) change at each of 100  
522 levels of task intensity between 0 and 1. Following a muscle's  
523 column from bottom to top shows the activation histograms  
524 for each magnitude of distal force and ending, naturally, with  
525 a spike about the unique value at maximal force production.

526 The flat areas in each surface plot (e.g. clearly visible  
527 for DI) represent muscle activation levels that are not valid  
528 for that task intensity. That is, there exist no valid muscle  
529 activation patterns that contain that muscle at that level, and  
530 thus no points are found there.

531 These plots show the nature and rate of convergence to the  
532 unique solution for maximal force output across muscles. We  
533 find that the histograms of activation levels for each muscle  
534 need not be symmetric, nor have the same shape (skewness  
535 and kurtosis) as the magnitude of the output force increases.  
536 For some muscles the convergence accelerates after 60% or  
537 80% of task intensity (as in LUM and EIP), while others  
538 converge monotonically along the entire progression (e.g. DI  
539 and PI). The peaks (i.e. modes) of each histogram at each  
540 task intensity represents the slice of the polytope that has  
541 the largest relative volume along that muscle dimension (i.e.,  
542 greatest frequency of that level of muscle activation across all  
543 valid solutions). Importantly, for most muscles (FDP, FDS,  
544 EIP, EDC, and LUM), the mode is not necessarily located at  
545 the same relative level of activation needed for maximal force  
546 output. That is, the histogram at high levels of force is not  
547 simply a shifted version of the histogram at low levels of force.  
548 The histograms for DI are the exception, whose modes seems  
549 to scale linearly with task intensity.

550 These histograms, in conjunction with the results in the  
551 parallel coordinate visualization, also demonstrate that the  
552 structure of feasible activation spaces cannot be inferred from  
553 their bounding boxes alone (i.e., upper and lower activation  
554 bounds for each muscle). An immediate example is how,  
555 for most task intensities, both EIP and LUM have similar  
556 lower and upper bounds near 0 and 1, respectively—yet their  
557 distributions are thoroughly distinct.



558  
559 **Fig. 6. PCA loadings change dramatically as task intensity increases** For each  
560 of 1,000 task intensities, we collected 1,000 points from the feasible activation space,  
561 and computed three principal components. Note that the signs of the loadings depend  
562 on the numerics of the PCA algorithm, and are subject to arbitrary flips in sign—  
563 thus for clarity we plot them such that FDP's loadings in PC1 are positive at all  
564 task intensities. Synergies at representative task intensities a, b, c in Fig. 5 differ.  
565 This reflects changes in the geometric structure of the feasible activation space as  
566 redundancy is lost.

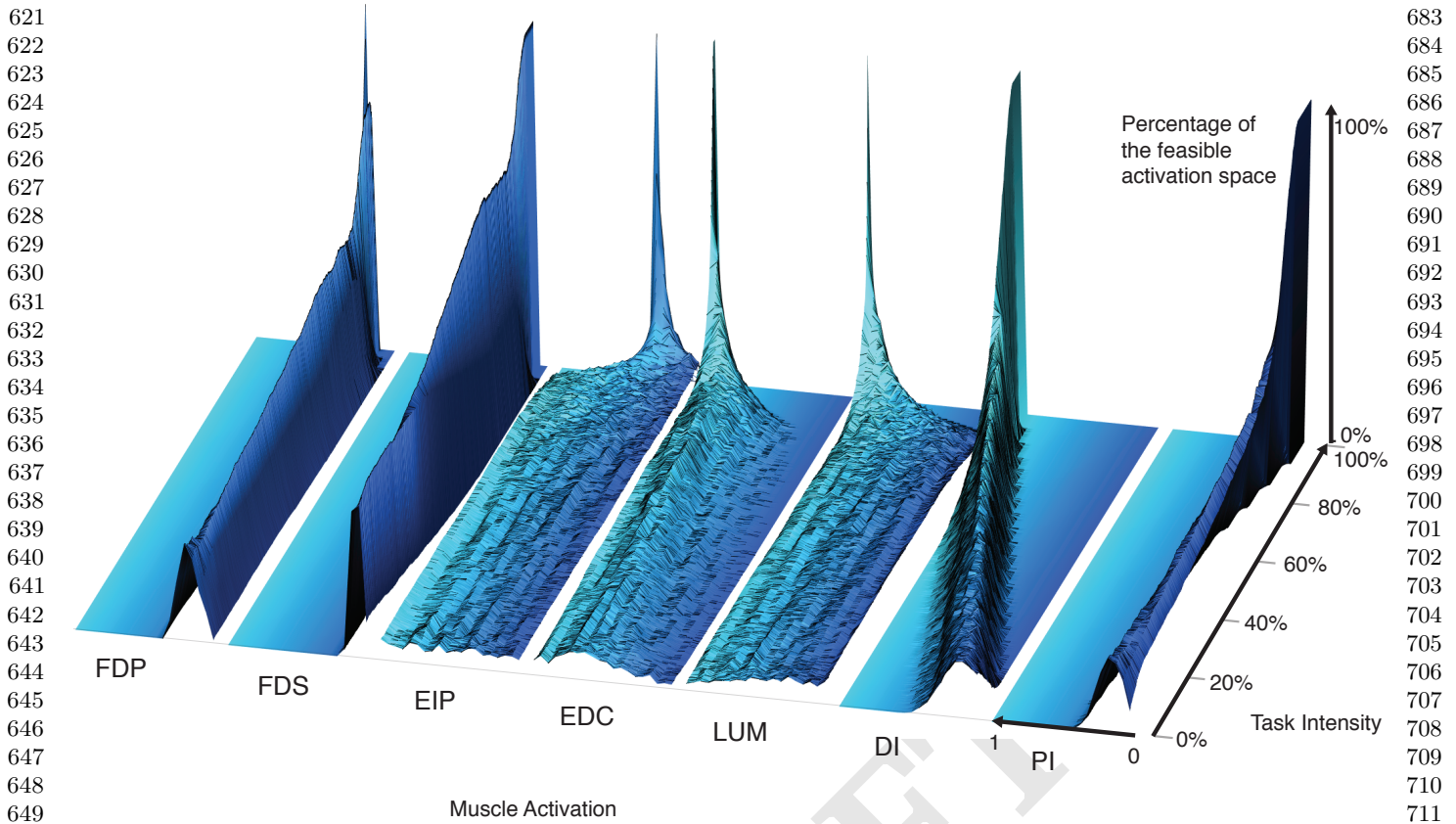


**Fig. 7. The within-muscle probabilistic structure of feasible muscle patterns across 1,000 levels of fingertip task intensity.** The changes in the breadth and height for each muscle reveal muscle-specific consequences of task intensity on their probability distributions. The cross-section of each density plot is the 50-bin histogram of activation for each muscle, at that task intensity. Height represents the percentage of solutions for that task. The axis going into the page indicates increasing fingertip task intensity up to 100% of maximal. Color is used to provide perspective.

## Discussion

**Summary.** Feasibility theory, as a conceptual and computational approach, is a means to pierce the curse of dimensionality to establish a physics-based ground truth for neuromuscular control. This practical approach can now characterize—in a complete way—the set of all valid ways to activate multiple muscles to produce a given task. Feasible activation spaces are, in fact, *the* neuromechanical landscapes upon which all neuromuscular learning, control, and performance must occur. Therefore, we provide an integrative and unifying perspective that demonstrates how today’s dominant theories of neuromuscular control are alternative approximations to feasible activation spaces from optimization, geometric, and probabilistic perspectives.

**The value of a cost function.** Optimization is the oldest computational approach to finding valid muscle activation patterns that produce limb function (e.g., (12)). While optimization is a reasonable hypotheses to explore neuromuscular control (15), some criticize it as mathematical abstraction that anthropomorphizes neurons with the ability to choose, evaluate and follow cost functions in high-dimensions (35, 36). There is an intimate relationship between optimization and feasible activation spaces (37). Optimization is analogous to finding a best solution in the dark—guided by repeated evaluations of a cost-function. Computing the feasible activation space is

then a means to ‘turn on the lights’ to see all possible valid solutions independently of cost (18). Our complete sampling of high-dimensional feasible activation spaces (38, 39) allows us to compare and contrast *families* of solutions instead of *individual* optimal solutions for a particular cost function. Fig. 3 demonstrates a complete description of families of valid coordination patterns and their relationship to alternative costs. Importantly, similar valid muscle activation patterns can have dissimilar costs, and vice versa.

Because these explorations can be done for alternative cost functions, they can provide quantitative overall descriptions of high-dimensional ‘cost landscapes.’ By not having to insist on (or settle for) individual optimal—or near-optimal—solutions, we now have the same ability the nervous system has to explore, compare and contrast multiple valid ways to coordinate muscles. Importantly, the relationships among valid muscle activation patterns emerge naturally from the physical properties of the limb and definition of the task. This cost-agnostic approach allows us to re-evaluate our assumptions about what the nervous system cares—and does not care—about. Lastly, this cost-agnostic approach also provides a powerful tool for inverse optimization, i.e., uncovering latent cost functions from data (40). Our comparison across cost functions using parallel coordinates is already a form of inverse optimization.

**Structure, correlation, and synergies.** The physical properties of the limb and definition of the task also define a low-

745 dimensional structure of the feasible activation space (18).  
746 Therefore, it is expected that experimental recordings of muscle  
747 activations during limb function will exhibit a dimensionality  
748 that is smaller than the number of muscles (1, 7). Thus,  
749 applying PCA to the points sampled from the feasible activation  
750 space also finds that few PCs can explain the variance in  
751 the data.

752 This application of PCA at increasing task intensities (i.e.,  
753 as muscle redundancy is lost) allows us to demonstrate—for  
754 the first time to our knowledge—several important features  
755 and limitations of dimensionality reduction. For example, we  
756 see that the aspect ratio (Fig. 5) and orientation (Fig. 6) of the  
757 feasible activation spaces change as their size shrinks (Fig. 7).  
758 Thus, such *descriptive* synergies extracted from limited exper-  
759 imental observations likely do not generalize well across task  
760 intensities. It is important to distinguish *descriptive* synergies  
761 (the dominant approach in the literature to extract synergies  
762 from experimental data using dimensionality reduction tech-  
763 niques such as PCA) from *prescriptive* synergies (those known  
764 to be implemented by the controller) (18).

765 This also has important consequences to motor control and  
766 learning. Producing force vectors at the endpoint of a finger  
767 or limb with accurate magnitude and direction are critical  
768 for versatile manipulation and locomotion (41–43). If a given  
769 synergy can produce such accurate force vectors only for a  
770 given task intensity (and thus inaccurate ones at other in-  
771 tensities), then the attractiveness of synergies to simplify the  
772 neuromuscular control of the limb is reduced. To compensate,  
773 the nervous system would need to learn, recall and implement  
774 specific synergies for each force level. In prior experimental  
775 work, we have shown that the nervous system produces accu-  
776 rate fingertip forces of different magnitudes by, instead, likely  
777 scaling a remembered muscle activation pattern to produce  
778 forces of different magnitudes, together with a full-dimensional,  
779 real-time error correction neural controller (44). Note that  
780 interpreting this experimental result still as a synergy-based  
781 approach would defeat the purpose of synergies as a means to  
782 simplify the control by reducing its dimensionality.  
783

784 Our results also show how experiments with realistically  
785 moderate numbers of participants and test trials likely do  
786 not contain sufficient data to produce robust estimates of de-  
787 scriptive synergies across task intensities. As per the curse  
788 of dimensionality, sampling uniformly at random from high-  
789 dimensional spaces is exponentially difficult. Thus, even for  
790 this anatomically complete 7-muscle finger model, PCA de-  
791 pends strongly on the number of independent observations,  
792 such as uncorrelated trials from one subject or different sub-  
793 jects. Figure 5 shows that 100 to 1,000 such ideal data points  
794 from a simulated ‘test subject’ are needed to produce accurate  
795 estimates of changes in PC1 and PC2 with task intensity (c.f.  
796 labels a vs. b vs. c). Future studies should explore how many  
797 experimental data points are sufficient from a given subject  
798 when recording from only a subset of the many (20+) muscles  
799 of human limbs in the presence of experimental noise, inherent  
800 stochasticity of EMG, and within- and between-subject vari-  
801 ability. Some studies have begun to ask subjects to explore  
802 different ways to perform a given task (45) (i.e., estimate  
803 the structure of the feasible activation space), but in practice  
804 such studies cannot likely collect sufficient data uniformly  
805 at random to obtain accurate estimates of the descriptive  
806 synergies (1). While our results suggest caution when inter-

807 preting synergies obtained experimentally, we underscore that  
808 dimensionality-reduction is a useful approach to capture global  
809 geometric properties of feasible activation spaces.  
810

811 **Toward probabilistic neuromuscular control.** Our results are  
812 particularly empowering for the emerging field of probabilistic  
813 neuromuscular control (8? –10). Suppose that the nervous  
814 system uses some form of probabilistic or Bayesian learning  
815 and control strategy. Such approach requires two enabling—  
816 and biologically feasible—elements: *trial-and-error iterative*  
817 *exploration*, and *memory-based exploitation* of the probability  
818 density functions used to approximate the feasible activation  
819 spaces (8). The parallel coordinate plots and histograms  
820 in Fig. 2 and 7 provide, to our knowledge, the first com-  
821 plete (38, 39) characterization of such multi-dimensional joint  
822 probability density functions for a realistic tendon-driven sys-  
823 tem performing a well-defined task.

824 These techniques and results now empower the study of  
825 fundamental aspects of probabilistic control. For example, an  
826 organism can only execute so many trial-and-error iterations  
827 during learning, likely too few to completely and exhaustively  
828 sample the high-dimensional feasible space of interest. This  
829 makes it much more likely that, by virtue of being more  
830 easily found, an organism will find and preferentially exploit  
831 the strong modes (i.e., narrow and high peaks in Figs. 3, 4,  
832 and 7) of the multi-dimensional probability density functions  
833 than any other region of feasible activation spaces. Thus,  
834 first, the maximal ranges of feasible activations described by  
835 the bounding box (29, 30) may have little practical bearing  
836 on how those tasks are learned and executed. And second,  
837 those same strong modes would represent strong attractors  
838 to create and reinforce motor habits. Habitual control has  
839 been proposed based on experimental and empirical data as an  
840 alternative to a strict optimization approach to neuromuscular  
841 control (35). Our work now provides the computational means  
842 to link habitual to probabilistic control. This allows us to  
843 generate testable hypotheses of how these motor habits are  
844 defined by the structure of the feasible activation space, how  
845 they are learned by the organism, and how difficult or easy it  
846 is to break out of them.

847 Thus, motor learning likely needs to proceed from adopting  
848 easily-found solutions independently of their cost, to using  
849 some low dimensional approximation to the gradient of the cost  
850 landscape, to then transitioning to less likely but potentially  
851 less costly subregions of the solutions space. This integrative  
852 perspective leads us to propose a hybrid approach to motor  
853 learning and execution where the practical limits on trial-and-  
854 error iterations are coupled with the low-dimensional structure  
855 of the solution space to enable some form of heuristic local  
856 optimization to create sub-optimal motor habits. Importantly,  
857 the organism performs strict optimization or synergy control at  
858 its peril. Take, for example, the case of a 2-dimensional feasible  
859 activation space embedded in 3-D, Fig. ??e. Taking a step from  
860 any one valid point to another valid point on the plane runs the  
861 risk of ‘falling off’ the solution space and failing at the task—a  
862 risk that is exponentially exacerbated in higher-dimensions.  
863 Thus, improvements in the neighborhood of a good solution  
864 necessarily risk task failure and potential injury. These are all  
865 arguments in support of the evolutionary and developmentally  
866 useful strategy to use good-enough control based on habit or  
867 sensorimotor memory rather than optimization (35, 46). This  
868 may explain why mass practice and coaches are so critical to

869	achieve elite athletic performance (47).	931
870		932
871	<b>Clinical implications.</b> This line of thinking has consequences 872 to neurorehabilitation. Neurological conditions disrupt feasible 873 activation spaces, be it by affecting anatomy of the limb, 874 muscle strength and independence with which muscles can be 875 controlled. Functional recovery following the disruption, if 876 not destruction, of the landscape of valid muscle activation 877 patterns requires re-learning existent, or building new, proba- 878 bility density functions. This occurs just when older adults 879 suffer from reduced perceptuo-motor learning rates (48).	933
880	A probabilistic landscape for neuromuscular function begins 881 to explain why neurorehabilitation in aging adults is so difficult 882 (e.g., (49)) and why motor learning in children takes thousands 883 of repetitions (50)—while also generating new rehabilitation 884 strategies, and testable hypotheses around them, that leverage 885 knowledge of the nature and structure of feasible activation 886 spaces.	934
887		935
888		936
889		937
890		938
891		939
892		940
893		941
894		942
895		943
896		944
897		945
898		946
899		947
900		948
901		949
902		950
903		951
904		952
905		953
906		954
907		955
908		956
909		957
910		958
911		959
912		960
913		961
914		962
915		963
916		964
917		965
918		966
919		967
920		968
921		969
922		970
923		971
924		972
925		973
926		974
927		975
928		976
929		977
930		978
931	where $H$ is the matrix of linear constraints defined by the muscu- loskeletal anatomy of the limb (29), $\mathbf{a}$ is the input vector of $n$ muscle activations, $\mathbf{f} \in \mathbb{R}^m$ is the $m$ -dimensional limb output ‘wrench’ (i.e., the forces and torques the finger can produce at the endpoint).	979
932	The output wrench, $m$ , is at most 6-dimensional (i.e., 3 forces 933 and 3 torques) depending on the number of kinematic degrees of 934 freedom of the limb, and usually $m < n$ because limbs have more 935 muscles than kinematic degrees of freedom (18). Muscles can only 936 pull, so elements of $\mathbf{a}$ cannot be negative, and are capped at 1 (i.e., 937 100% of maximal muscle activation).	980
938	What are the muscle coordination patterns that produce a given 939 task? As explained in (18), the task of producing a static fingertip 940 force vector is defined by specifying the desired values for the 941 elements of the endpoint forces and torques of $\mathbf{w}$ . Each such 942 constraint equation defines a hyperplane of dimension $n-1$ , and their 943 combination defines the task completely. The <i>feasible activation</i> 944 space of the task, if it is well posed (37), is defined by the points $\mathbf{a}$ 945 that lie within the $n$ -cube and at the intersection of all constraint 946 hyperplanes.	981
947	Geometrically speaking, the feasible activation space is a $(n-m)$ - 948 dimensional convex polytope $P$ embedded in $\mathbb{R}^n$ that contains all $n$ - 949 dimensional muscle coordination patterns (i.e., points $\mathbf{a}$ ) that satisfy 950 all constraints, and therefore can produce the task. Increasing 951 task specificity by adding more constraints naturally decreases 952 the dimensionality and changes the size and shape of the feasible 953 activation space (20, 30, 51).	982
954	<b>The Hit-and-Run algorithm uniformly samples from feasible activa- 955 tion spaces</b> Calculating the geometric properties of convex poly- 956 topes in high dimensions is computationally challenging. Taking 957 the generalized concept of an $n$ -dimensional volume as an example 958 of a geometric property of interest, the exact volume computations 959 for $n$ -dimensional polytopes is known to be tractable only in a poly- 960 nomial amount of time (i.e., $\#P$ -hard) (52). Currently available 961 volume algorithms can only handle polytopes embedded in small 962 dimensions like 10 or slightly more (53). Studying vertebrate limbs 963 in general, however, can require including several dozen muscles, 964 such as our studies of a 17-muscle human arm and a 31-muscle cat 965 hindlimb model (29); and other limb models have over 40 muscles 966 such as (1, 54–56).	983
967	Similar difficulties arise when computing other geometric proper- 968 ties such as the shape and aspect ratio of $P$ in high dimensions. We 969 and others have described polytopes $P$ by their bounding box (i.e., 970 the range of values in every dimension) (30, 33), but that singularly 971 overestimates the shape and volume of the feasible activation space 972 as discussed in (29). Take Fig. ??e as an example, where the bound- 973 ing box of the 2-dimensional polygon has a volume—even though a 974 plane has zero volume—, and can be almost as large as the positive 975 unit cube itself. Similar problems arise in the interpretation of the 976 inscribed and circumscribed ball (57).	984
977	We applied the Hit-and-Run method to sample points from the 978 feasible activation space—a method that is evaluated and justified in 979 (18?). This complete probabilistic method describes the structure 980 of feasible activation spaces $P$ with a set of uniformly-at-random 981 muscle activation patterns that produce the same wrench. This 982 enables us to derive descriptive statistics, histograms, and point 983 densities of the set of valid muscle activation patterns $\mathbf{a}$ uniformly 984 sampled from the polytope. To do so, we use the Hit-and-Run 985 method. We have presented a detailed explanation of the theory 986 (In Chapter 9 of (18)), and have justified the utility of this method 987 on tendon-driven models of the index finger (? ).	985
988		986
989		987
990		988
991		989
992		990
993		991
994		992
995		993
996		994
997		995
998		996
999		997
1000		998
1001		999
1002		1000
1003		1001
1004		1002
1005		1003
1006		1004
1007		1005
1008		1006
1009		1007
1010		1008
1011		1009
1012		1010
1013		1011
1014		1012
1015		1013
1016		1014
1017		1015
1018		1016
1019		1017
1020		1018
1021		1019
1022		1020
1023		1021
1024		1022
1025		1023
1026		1024
1027		1025
1028		1026
1029		1027
1030		1028
1031		1029
1032		1030
1033		1031
1034		1032
1035		1033
1036		1034
1037		1035
1038		1036
1039		1037
1040		1038
1041		1039
1042		1040
1043		1041
1044		1042
1045		1043
1046		1044
1047		1045
1048		1046
1049		1047
1050		1048
1051		1049
1052		1050
1053		1051
1054		1052
1055		1053
1056		1054
1057		1055
1058		1056
1059		1057
1060		1058
1061		1059
1062		1060
1063		1061
1064		1062
1065		1063
1066		1064
1067		1065
1068		1066
1069		1067
1070		1068
1071		1069
1072		1070
1073		1071
1074		1072
1075		1073
1076		1074
1077		1075
1078		1076
1079		1077
1080		1078
1081		1079
1082		1080
1083		1081
1084		1082
1085		1083
1086		1084
1087		1085
1088		1086
1089		1087
1090		1088
1091		1089
1092		1090
1093		1091
1094		1092
1095		1093
1096		1094
1097		1095
1098		1096
1099		1097
1100		1098
1101		1099
1102		1100
1103		1101
1104		1102
1105		1103
1106		1104
1107		1105
1108		1106
1109		1107
1110		1108
1111		1109
1112		1110
1113		1111
1114		1112
1115		1113
1116		1114
1117		1115
1118		1116
1119		1117
1120		1118
1121		1119
1122		1120
1123		1121
1124		1122
1125		1123
1126		1124
1127		1125
1128		1126
1129		1127
1130		1128
1131		1129
1132		1130
1133		1131
1134		1132
1135		1133
1136		1134
1137		1135
1138		1136
1139		1137
1140		1138
1141		1139
1142		1140
1143		1141
1144		1142
1145		1143
1146		1144
1147		1145
1148		1146
1149		1147
1150		1148
1151		1149
1152		1150
1153		1151
1154		1152
1155		1153
1156		1154
1157		1155
1158		1156
1159		1157
1160		1158
1161		1159
1162		1160
1163		1161
1164		1162
1165		1163
1166		1164
1167		1165
1168		1166
1169		1167
1170		1168
1171		1169
1172		1170
1173		1171
1174		1172
1175		1173
1176		1174
1177		1175
1178		1176
1179		1177
1180		1178
1181		1179
1182		1180
1183		1181
1184		1182
1185		1183
1186		1184
1187		1185
1188		1186
1189		1187
1190		1188
1191		1189
1192		1190
1193		1191
1194		1192
1195		1193
1196		1194
1197		1195
1198		1196
1199		1197
1200		1198
1201		1199
1202		1200
1203		1201
1204		1202
1205		1203
1206		1204
1207		1205
1208		1206
1209		1207
1210		1208
1211		1209
1212		1210
1213		1211
1214		1212
1215		1213
1216		1214
1217		1215
1218		1216
1219		1217
1220		1218
1221		1219
1222		1220
1223		1221
1224		1222
1225		1223
1226		1224
1227		1225
1228		1226
1229		1227
1230		1228
1231		1229
1232		1230
1233		1231
1234		1232
1235		1233
1236		1234
1237		1235
1238		1236
1239		1237
1240		1238
1241		1239
1242		1240
1243		1241
1244		1242
1245		1243
1246		1244
1247		1245
1248		1246
1249		1247
1250		1248
1251		1249
1252		1250
1253		1251
1254		1252
1255		1253
1256		1254
1257		1255
1258		1256
1259		1257
1260		1258
1261		1259
1262		1260
1263		1261
1264		1262
1265		1263
1266		1264
1267		1265
1268		1266
1269		1267
1270		1268
1271		1269
1272		1270
1273		1271
1274		1272
1275		1273
1276		1274
1277		1275
1278		1276
1279		1277
1280		1278
1281		1279
1282		1280
1283		1281
1284		1282
1285		1283
1286		1284
1287		1285
1288		1286
1289		1287
1290		1288
1291		1289
1292		1290
1293		1291
1294		1292
1295		1293
1296		1294
1297		1295
1298		1296
1299		1297
1300		1298
1301		1299
1302		1300
1303		1301
1304		1302
1305		1303
1306		1304
1307		1305
1308		

993 where

$$\mathbf{a} = \begin{pmatrix} a_{FDP} \\ a_{FDS} \\ a_{EIP} \\ a_{EDC} \\ a_{LUM} \\ a_{DI} \\ a_{PI} \end{pmatrix} \quad [5]$$

1000 In Cartesian coordinates, the 4-D output wrench corresponds to  
1001 the anatomical directions shown in Fig. 1e.

$$\mathbf{w} = \begin{pmatrix} f_x \\ f_y \\ f_z \\ \tau_x \end{pmatrix} = \begin{pmatrix} f_{radial} \\ f_{distal} \\ f_{palmar} \\ \tau_{radial} \end{pmatrix} \quad [6]$$

1002 The biomechanical model  $H$  includes three serial links articulated  
1003 by four kinematic degrees of freedom (ad-abduction, flexion-  
1004 extension at the metacarpophalangeal joint, and flexion-extension at  
1005 the proximal and distal interphalangeal joints). The action of each  
1006 of the seven muscles (FDP: *flexor digitorum profundus*, FDS: *flexor  
1007 digitorum superficialis*, EIP: *extensor indicis proprius*, EDC: *exten-  
1008 sor digitorum communis*, LUM: *lumbrical*, DI: *dorsal interosseous*,  
1009 and PI: *palmar interosseous*) on each joint to produce torque is  
1010 given by the moment arm matrix  $R \in \mathbb{R}^{4 \times 7}$ . Lastly,  $J \in \mathbb{R}^{4 \times 4}$   
1011 and  $F_0 \in \mathbb{R}^{7 \times 7}$  are the Jacobian of the fingertip with 4 kinematic  
1012 degrees of freedom, and the diagonal matrix containing the maximal  
1013 strengths of the seven muscles, respectively (18, 44). The finger  
1014 posture was defined to be 0° ad-abduction and 45° flexion at the  
1015 metacarpophalangeal joint, and 45° and 10° flexion, respectively,  
1016 at the proximal and distal interphalangeal joints.

1017 **Feasible activation space for a static fingertip force task** Our goal  
1018 is to find the family of all feasible muscle activation patterns that  
1019 can produce a given task. In particular, the task we explored is  
1020 producing various magnitudes of a submaximal static force in the  
1021 distal direction  $f_{distal}$  — in the absence of any  $\tau_{radial}$ , shown in  
1022 Fig. 1f. Therefore the feasible activation space is a polytope  $P$  in  
1023 7-dimensional activation space that meets the following four linear  
1024 constraints in  $\mathbf{a}$  (18, 21, 44)

$$f_{radial} = 0 \quad [7]$$

$$f_{distal} = \text{desired magnitude as \% of maximal} \quad [8]$$

$$f_{palmar} = 0 \quad [9]$$

$$\tau_{palmar} = 0 \quad [10]$$

1025 These four constraints on the static output of the finger yield a 3-  
1026 dimensional (i.e.,  $7 - 4 = 3$ ) polytope  $P$  embedded in 7-dimensional  
1027 activation space. For details on how to create such models, apply  
1028 task constraints and find such polytopes via vertex enumeration  
1029 methods, see (18).

1030 For the index finger model used in this paper, the published  
1031 maximal feasible force in the distal direction is 28.81 Newtons. We  
1032 defined the normalized desired distal task intensity as a value ranging  
1033 between 0 and 1, i.e., each submaximal force can be produced by  
1034 any of the points contained in its corresponding feasible activation  
1035 space. For the production of a maximal force, the feasible activation  
1036 space shrinks to a single point (12, 19, 37, 44).

#### 1037 Analysis of feasible activation spaces.

1038 **Parallel coordinates visualization shows the location of all points  
1039 across all dimensions** Parallel coordinates are a common graphical  
1040 approach to visualize interactions among high-dimensional data  
1041 (59, 60). To demonstrate this visualization method, consider the  
1042 results of the simple 3-dimensional example shown in Fig. 2. We  
1043 begin by drawing  $n$  parallel vertical lines for each of the dimensions  
1044  $n$  (i.e., 3 muscles). With the axis limits of each line set between 0  
1045 and 1, each point (Fig. 2a) is then represented by connecting their  
1046 coordinates by  $n - 1$  lines as shown in Fig. 2b.

1047 **Neural and metabolic cost functions** As mentioned in the Introduction,  
1048 the field of neuromuscular control has a long historical tradition of using optimization to find muscle activation patterns

1049 that minimize effort, which requires the (often contentious) definition  
1050 of cost functions (12, 13, 16, 19). Therefore, we used four representative  
1051 cost functions to calculate the relative fitness of each of the muscle activation  
1052 patterns sampled—in effect also calculating the fitness landscape across all possible solutions. The cost functions are defined at the level of neural effort ( $L_1$ , and  $L_2$  norms);  
1053 and at the level of metabolic cost, thought to be approximated by neural drive weighted by the strength of each muscle ( $L_1^w$  and  $L_2^w$  norms) (13, 16).

1054 To visualize the costs associated with each valid muscle coordination  
1055 pattern, we simply added four vertical lines at the far right of the parallel coordinates plot, one for each cost function, Fig. 2c. The variables  $a_i$  and  $F_{0i}$  represent the activation of the  $i^{th}$  muscle  
1056 in a given muscle activation pattern, and the maximal strength of each muscle (13, 16). Maximal muscle strengths are approximated  
1057 by multiplying each muscle's physiological cross-sectional area, in  $\text{cm}^2$ , by the maximal active muscle stress of mammalian muscle,  
1058 35  $\text{N}/\text{cm}^2$  (61). These four cost functions are but four examples as the literature contains many others as any investigator is in fact  
1059 free to chose any cost function deemed relevant to their study.

1060 **Histograms of the activation level of each muscle across all valid solutions** Muscle-by-muscle histograms are another straightforward  
1061 way to visualize the many points sampled from the convex polytope.  
1062 Histograms are particularly helpful because they are approximations  
1063 to probability density functions. They visualize the relative number  
1064 of solutions (i.e., density of solutions) that required a particular  
1065 level of activation from a particular muscle within its range of [0, 1].  
1066 In addition, the upper and lower bounds of the histograms show,  
1067 in fact, the size of the side of the bounding box of the polytope in  
1068 every dimension (i.e., for independently controlled muscle).

1069 **Dimensionality reduction** Investigators have repeatedly reported  
1070 that electromyographical signals (i.e., experimental estimates of  
1071 muscle activation patterns) tend to exhibit strong correlations with  
1072 one another. In these experimental descriptions of dimensionality  
1073 reduction of neuromuscular control, only few independent functions—  
1074 sometimes called synergies—suffice to explain the majority of the  
1075 variability in the observed muscle activation patterns (1–4, 6, 7, 62).  
1076 Principal components analysis (PCA) is a widely used technique to  
1077 extract these few independent basis functions (correlation vectors  
1078 called principal components, PCs) from high-dimensional data (63).  
1079 In this case, PCs are often called the experimental representations  
1080 of synergies of neural origin (1).

1081 Therefore, we also applied PCA to points (i.e., muscle coordination  
1082 patterns) sampled from the feasible activation space at each force level.  
1083 This provides the PCs that describe the correlations among valid muscle activation patterns for a given task. For example,  
1084 the feasible activation space  $P$  in Fig. ??e is a 2-dimensional polygon embedded in 3-dimensional activation space. Thus, applying  
1085 PCA to points sampled from the polygon will extract 2 synergies (i.e., 3-dimensional correlation vectors PC1 and PC2) that wholly  
1086 explain the feasible activation space. By extension, in the case of  
1087 fingertip force production in Fig. 1, the feasible activation space is  
1088 a 3-dimensional polytope embedded of the 7-dimensional activation  
1089 space. And PCA should extract, by construction, as many synergies  
1090 as there are dimensions in the feasible activation space. For static  
1091 force production with the index fingertip (i.e., 7 muscles and 4  
1092 constraints), we know that 3 principal components should describe  
1093 100% of the variance in points sampled from the feasible activation  
1094 space (i.e., 7-dimensional correlation vectors PC1, PC2, and PC3).

1095 Applying PCA to our data allows us to test whether and how  
1096 its results change when applied to feasible activation spaces for  
1097 different magnitudes of fingertip force. We applied PCA to feasible  
1098 activation spaces for fingertip task intensities ranging from 0 to 90%  
1099 of maximal. We compare both the variance explained by each PC  
1100 and their vector direction (i.e., the ‘loadings’ or correlations among  
1101 muscle (64)) as the force level increases. Lastly, we tested whether  
1102 our PCA results are sensitive to the number of points sampled  
1103 from each feasible activation space. This is important because  
1104 experimental studies test 10 or so subjects in practice, which may  
1105 be too few when sampling from high-dimensional spaces.

1106 **ACKNOWLEDGMENTS.** Research reported in this publication  
1107 was supported by the National Institute of Arthritis and Muscu-  
1108

- 1117 loskeletal and Skin Diseases of the National Institutes of Health  
1118 (NIH) under Awards Number R01 AR-050520 and R01 AR-052345  
1119 to FVC, and the Swiss National Science Foundation (SNF Project  
1120 200021\_150055 / 1) to BG, KF and FVC. The content is solely the  
1121 responsibility of the authors and does not necessarily represent the  
1122
- 1123 official views of the SNSF or the NIH. We thank Komei Fukuda for  
1124 his integral support in designing this research collaboration. We  
1125 thank J Pugliesi, T Kim, C Lim, A Baugus, P Vachhani, and A  
1126 Boling for extending the scientific rigor of this work through reviews,  
1127 documentation, and code  
1128
- 1129
- 1130 1. Kutch J, Valero-Cuevas F (2012) Challenges and new approaches to proving the existence  
1131 of muscle synergies of neural origin. *PLoS Computational Biology* 8(5):e1002434.
  - 1132 2. Steele KM, Tresch MC, Perreault EJ (2013) The number and choice of muscles impact the  
1133 results of muscle synergy analyses. *Frontiers in computational neuroscience* 7.
  - 1134 3. Bizzi E, Cheung VC (2013) The neural origin of muscle synergies. *Frontiers in computational  
1135 neuroscience* 7.
  - 1136 4. Dingwell JB, John J, Cusumano JP (2010) Do humans optimally exploit redundancy to control  
1137 step variability in walking? *PLoS computational biology* 6(7):e1000856.
  - 1138 5. Rácz K, Valero-Cuevas FJ (2013) Spatio-temporal analysis reveals active control of both  
1139 task-relevant and task-irrelevant variables. *Frontiers in computational neuroscience* 7.
  - 1140 6. Steele KM, Tresch MC, Perreault EJ (2015) Consequences of biomechanically constrained  
1141 tasks in the design and interpretation of synergy analyses. *Journal of neurophysiology*  
1142 113(7):2102–2113.
  - 1143 7. Alessandro C, Delis I, Nori F, Panzeri S, Berret B (2013) Muscle synergies in neuroscience  
1144 and robotics: from input-space to task-space perspectives. *Frontiers in computational neuro-  
1145 science* 7.
  - 1146 8. Kording KP, Wolpert DM (2004) Bayesian integration in sensorimotor learning. *Nature*  
1147 427(6971):244–247.
  - 1148 9. Kording KP (2014) Bayesian statistics: relevant for the brain? *Current Opinion in Neurobiology*  
1149 25:130 – 133. Theoretical and computational neuroscience.
  - 1150 10. Berniker M, O'Brien MK, Kording KP, Ahmed AA (2013) An examination of the generalizability  
1151 of motor costs. *PLoS one* 8(1):e53759.
  - 1152 11. Sanger TD (2011) Distributed control of uncertain systems using superpositions of linear  
1153 operators. *Neural computation* 23(8):1911–1934.
  - 1154 12. Chao E, An K (1978) Graphical interpretation of the solution to the redundant problem in  
1155 biomechanics. *Journal of Biomechanical Engineering* 100:159–67.
  - 1156 13. Prilutsky BI (2000) Muscle coordination: the discussion continues. *Motor Control* 4(1):97–116.  
1157 0 1087-1640 Journal article.
  - 1158 14. Scott SH (2004) Optimal feedback control and the neural basis of volitional motor control.  
1159 *Nature Reviews Neuroscience* 5(7):532–546.
  - 1160 15. Todorov E, Jordan MI (2002) Optimal feedback control as a theory of motor coordination.  
1161 *Nature neuroscience* 5(11):1226–1235.
  - 1162 16. Crowninshield R, Brand R (1981) A physiologically based criterion of muscle force prediction  
1163 in locomotion. *Journal of Biomechanics* 14(11):793–801.
  - 1164 17. Higginson J, Neptune R, Anderson F (2005) Simulated parallel annealing within a neighbor-  
1165 hood for optimization of biomechanical systems. *Journal of biomechanics* 38(9):1938–1942.
  - 1166 18. Valero-Cuevas FJ (2015) *Fundamentals of Neuromechanics*, Biosystems and Biorobotics.  
1167 SpringerVerlag London Vol. 8.
  - 1168 19. Spoor C (1983) Balancing a force on the fingertip of a two-dimensional finger model without  
1169 intrinsic muscles. *Journal of Biomechanics* 16(7):497–504.
  - 1170 20. Kuo A, Zajac F (1993) Human standing posture: multi-joint movement strategies based on  
1171 biomechanical constraints. *Progress in Brain Research* 97:349–358.
  - 1172 21. Valero-Cuevas FJ, Zajac FE, Burgar CG (1998) Large index-fingertip forces are produced by  
1173 subject-independent patterns of muscle excitation. *Journal of Biomechanics* 31:693–703.
  - 1174 22. Gallego JA, Perich MG, Miller LE, Solla SA (2017) Neural manifolds for the control of move-  
1175 ment. *Neuron* 94(5):978–984.
  - 1176 23. Bellman R, Osborne H (1958) Dynamic programming and the variation of green's functions.  
1177 *Journal of Mathematics and Mechanics* pp. 81–85.
  - 1178 24. Bellman RE (2015) *Adaptive control processes: a guided tour*. (Princeton university press).
  - 1179 25. Avis D, Fukuda K (1992) A pivoting algorithm for convex hulls and vertex enumeration of  
1180 arrangements and polyhedra. *Discrete & Computational Geometry* 8(3):295–313.
  - 1181 26. Valero-Cuevas FJ, Hoffmann H, Kurze MU, Kutch JJ, Theodorou EA (2009) Computational  
1182 models for neuromuscular function. *IEEE Reviews in Biomedical Engineering* (2) October p.  
1183 110n135.
  - 1184 27. Theodorou E, Valero-Cuevas FJ (2010) Optimality in neuromuscular systems in *Engineering  
1185 in Medicine and Biology Society (EMBC), 2010 Annual International Conference of the IEEE*.  
1186 (IEEE), pp. 4510–4516.
  - 1187 28. Scholz JP, Schöner G (1999) The uncontrolled manifold concept: identifying control variables  
1188 for a functional task. *Exp Brain Res* 126:289–306.
  - 1189 29. Valero-Cuevas FJ, Cohn BA, Yingvason HF, Lawrence EL (2015 In Press) Exploring the high-  
1190 dimensional structure of muscle redundancy via subject-specific and generic musculoskeletal  
1191 models. *Journal of Biomechanics* doi:10.1016/j.jbiomech.2015.04.026.
  - 1192 30. Sohn MH, McKay JL, Ting LH (2013) Defining feasible bounds on muscle activation in a  
1193 redundant biomechanical task: practical implications of redundancy. *Journal of biomechanics*  
1194 46(7):1363–1368.
  - 1195 31. Venkadesan M, Valero-Cuevas FJ (2008) Neural control of motion-to-force transitions with  
1196 the fingertip. *J. Neurosci.* 28:1366–1373.
  - 1197 32. Valero-Cuevas FJ, Towles JD, Hertz VR (2000) Quantification of fingertip force reduction  
1198 in the forefinger following simulated paralysis of extensor and intrinsic muscles. *Journal of  
1199 biomechanics* 33(12):1601–1609.
  - 1200 33. Kutch JJ, Valero-Cuevas FJ (2011) Muscle redundancy does not imply robustness to muscle  
1201 dysfunction. *Journal of Biomechanics* 44(7):1264–1270.
  - 1202 34. Valero-Cuevas FJ (2000) Predictive modulation of muscle coordination pattern magnitude  
1203 scales fingertip force magnitude over the voluntary range. *J. Neurophysiol.* 83:1469–1479.
  - 1204 35. De Rugy A, Loeb GE, Carroll TJ (2012) Muscle coordination is habitual rather than optimal.  
1205 *The Journal of Neuroscience* 32(21):7384–7391.
  - 1206 36. Loeb G (2012) Optimal is not good enough. *Biological Cybernetics* 106(11-12):757–765.
  - 1207 37. Chvatal V (1983) *Linear programming*. (Macmillan).
  - 1208 38. Smith RL (1984) Efficient monte carlo procedures for generating points uniformly distributed  
1209 over bounded regions. *Operations Research* 32(6):1296–1308.
  - 1210 39. Lovász L (1999) Hit-and-run mixes fast. *Mathematical Programming* 86(3):443–461.
  - 1211 40. Tsirakos D, Baltzopoulos V, Bartlett R (1997) Inverse optimization: functional and physiolog-  
1212 ical considerations related to the force-sharing problem. *Critical Reviews™ in Biomedical  
1213 Engineering* 25(4-5).
  - 1214 41. Cole KJ (2006) Age-related directional bias of fingertip force. *Experimental brain research*  
1215 175(2):285–291.
  - 1216 42. Valero-Cuevas FJ, Zajac FE, Burgar CG (1998) Large index-fingertip forces are produced by  
1217 subject-independent patterns of muscle excitation. *Journal of Biomechanics* 31(8):693–704.
  - 1218 43. Donegan JM, Shipman DW, Kram R, Kuo AD (2004) Mechanical and metabolic requirements  
1219 for active lateral stabilization in human walking. *Journal of biomechanics* 37(6):827–835.
  - 1220 44. Valero-Cuevas FJ (2000) Predictive modulation of muscle coordination pattern magnitude  
1221 scales fingertip force magnitude over the voluntary range. *J Neurophysiol* 83(3):1469–1479.
  - 1222 45. Berger DJ, d'Avella A (2014) Effective force control by muscle synergies. *Frontiers in compu-  
1223 tational neuroscience* 8.
  - 1224 46. Fu Q, Santello M (2012) Context-dependent learning interferes with visuomotor transforma-  
1225 tion for manipulation planning. *Journal of Neuroscience* 32(43):15086–15092.
  - 1226 47. Gladwell M (2008) *Outliers: The story of success*. (Hachette UK).
  - 1227 48. Coats RO, Wilson AD, Snapp-Chidts W, Fath AJ, Bingham GP (2014) The 50s cliff: perceptuo-  
1228 motor learning rates across the lifespan. *PLoS one* 9(1):e85758.
  - 1229 49. Hardwick RM, Rajan VA, Bastian AJ, Krakauer JW, Celnik PA (2016) Motor learning in stroke:  
1230 Trained patients are not equal to untrained patients with less impairment. *Neurorehabilitation  
and Neural Repair* p. 1545968316675432.
  - 1231 50. Adolph KE, et al. (2012) How do you learn to walk? thousands of steps and dozens of falls  
1232 per day. *Psychological science* 23(11):1387–1394.
  - 1233 51. Inouye JM, Valero-Cuevas FJ (2016) Muscle synergies heavily influence the neural control of  
1234 arm endpoint stiffness and energy consumption. *PLoS Comput Biol* 12(2):e1004737.
  - 1235 52. Dyer M, Frieze A, Kannan R (1989) A random polynomial time algorithm for approximating the  
1236 volume of convex bodies. *Proc. of the 21st annual ACM Symposium of Theory of Computing*  
pp. 375–381.
  - 1237 53. Büeler B, Enge A, Fukuda K (2000) Exact volume computation for polytopes: A practical  
1238 study. *Polytopes: Combinatorics and Computation* 29:131–154.
  - 1239 54. Arnold EM, Ward SR, Lieber RL, Delp SL (2010) A model of the lower limb for analysis of  
1240 human movement. *Annals of biomedical engineering* 38(2):269–279.
  - 1241 55. Hammer SR, Seth A, Delp SL (2010) Muscle contributions to propulsion and support during  
1242 running. *Journal of biomechanics* 43(14):2709–2716.
  - 1243 56. De Sapio V, Earl D, Green R, Saul K (2014) Human factors simulation using demographically  
1244 tuned biomechanical models in *Proceedings of the Human Factors and Ergonomics Society Annual  
Meeting*. (SAGE Publications Sage CA: Los Angeles, CA), Vol. 58, pp. 944–948.
  - 1245 57. Inouye JM, Kutch JJ, Valero-Cuevas FJ (2014) Optimizing the topology of tendon-driven fin-  
1246 gers: Rationale, predictions and implementation in *The Human Hand as an Inspiration for Robot  
Hand Development*. (Springer), pp. 247–266.
  - 1247 58. Valero-Cuevas F, Hoffmann H, Kurze M, Kutch J, Theodorou E (2009) Computational models  
1248 for neuromuscular function. *Biomedical Engineering, IEEE Reviews in* 2:110–135.
  - 1249 59. Bachynskyi M, Oulasvirta A, Palmas G, Weinkauf T (2013) Biomechanical simulation in the  
1250 analysis of aimed movements in *CHI'13 Extended Abstracts on Human Factors in Computing  
Systems*. (ACM), pp. 277–282.
  - 1251 60. Krekel PR, et al. (2010) Visual analysis of multi-joint kinematic data in *Computer Graphics  
Forum*. (Wiley Online Library), Vol. 29, pp. 1123–1132.
  - 1252 61. Zajac FE (1993) Muscle coordination of movement: a perspective. *J Biomech* 26 Suppl  
1:109–124.
  - 1253 62. Krishnamoorthy V, Goodman S, Zatsiorsky V, Latash ML (2003) Muscle synergies during  
1254 shifts of the center of pressure by standing persons: identification of muscle modes. *Biologi-  
cal cybernetics* 89(2):152–161.
  - 1255 63. Clewley RH, Guckenheimer JM, Valero-Cuevas FJ (2008) Estimating effective degrees of  
1256 freedom in motor systems. *IEEE Trans Biomed Eng* 55:430–442.
  - 1257 64. Valero-Cuevas FJ, Klamroth-Marganska V, Winstein CJ, Riener R (2016) Robot-assisted and  
1258 conventional therapies produce distinct rehabilitative trends in stroke survivors. *Journal of  
1259 neuroengineering and rehabilitation* 13(1):92.